A coupled discrete element - lattice Boltzmann method to investigate internal erosion in soil

Franck Lominé, Luc Sibille, Didier Marot

A COUPLED DISCRETE ELEMENT – LATTICE BOLTZMANN METHOD TO INVESTIGATE INTERNAL EROSION IN SOIL

Franck Lominé
GeM laboratory, University of Nantes ECN CNRS IUT de St-Nazaire, BP 420, 44606 Saint-Nazaire Cedex, France

Luc Sibille
GeM laboratory, University of Nantes ECN CNRS IUT de St-Nazaire, BP 420, 44606 Saint-Nazaire Cedex, France

Didier Marot
GeM laboratory, University of Nantes ECN CNRS IUT de St-Nazaire, BP 420, 44606 Saint-Nazaire Cedex, France

ABSTRACT: *In this paper, we present a coupled Discrete Element (DE) and Lattice Boltzmann (LB) method to model fluid-solid interactions. This method is applied to study and model a two-dimensional piping erosion through a set-up inspired by the Hole Erosion Test (HET). In this work, we mainly focus on grain detachments under hydraulic loading. Simulation results show that the erosion law classically used in such experiments, can be retrieved with our model. It illustrates that such coupled systems can be investigated with the LB-DE approach developed in this work. This approach is a promising tool which is well designed to perform such investigations at the grain scale.*

1 INTRODUCTION

Internal erosion in soil can be defined by the migration of solid particles due to interstitial water flow. Such migrations can result in the degradation of hydraulic and mechanical properties of soils which can induce structure breakages (Foster et al. 2000). During internal erosion process, particles can be detached, transported and filtered. The full description of internal erosion is nowadays an interesting research project but remains a great challenge due to the variety and the complexity of phenomena involved. In this paper, we focus our interest on particle detachment due to hydraulic loading through direct simulations of piping erosion. Our numerical set-up is inspired by the Hole Erosion Test (HET) (Wan & Fell 2004; Pham 2008; Regazzoni 2009), commonly used in civil engineering to characterize erodability of soils. In this paper, we develop and use a coupling between the Discrete Element (DE) and Lattice Boltzmann (LB) methods. Contact interactions between grains are described with the DE method, whereas fluid flow is computed at a very small scale (smaller than the grain scale) with the LB method. Solid-fluid interactions are described along each grain boundary by the coupling between the two methods without additional parameters.
In the first part of this paper, we present the numerical model and the set-up of our simulations used to model piping erosion. Then, preliminary results of this study will be presented in a second part.

2 NUMERICAL MODEL AND SET-UP

2.1 Discrete Element method (DE)

We use the Discrete Element (DE) method as introduced by Cundall & Strack (1979). Particles move according to Newton's law and two particles in contact can slightly overlap each other. Hence, contact interaction forces are computed, for each pair of particles in contact, with a contact law depending on the overlap between particles. In this paper, we use a cohesive frictional contact law as illustrated in Fig. 1. In the normal direction to the tangent contact plane, the interaction law is purely elastic and expressed as $F_n = k_n\,\delta_n$, where F_n is the normal contact force, k_n the normal stiffness, and δ_n the normal overlap between particles. We allow tensile normal forces for $F_n \geq C_n$, where C_n is a normal contact cohesion. If $F_n < C_n$ failure occurs and the contact is lost. In this model, we assume that compressive forces F_n are counted positively therefore C_n takes usually negative values.

Along the tangential direction (included in the contact plane), we use an elastic-plastic interaction law which follows the Coulomb's friction law. In the elastic regime, the tangential interaction force is expressed as $\Delta F_s = -k_s\,\Delta u_s$, where ΔF_s, k_s and Δu_s are respectively the shear force increment, the shear stiffness and the increment of the tangential relative displacement of particles at contact. When $|F_s| > F_n\,\tan(\Phi) + C_s$, where Φ and C_s are respectively the contact friction angle and the shear cohesion, sliding in tangential direction occurs and the contact becomes purely frictional (i.e. $C_n = C_s = 0$).

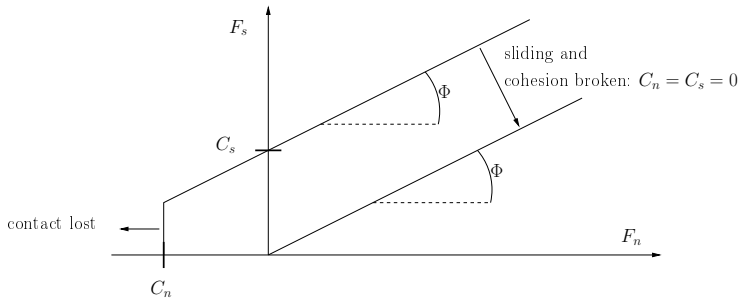

Fig. 1. Cohesive frictional contact law used in the Discrete Element method.

The Discrete Element method uses an explicit time integration of Newton's second law to update positions and velocities (in translation and in rotation) of each solid particle. Consequently, the numerical stability of the time integration scheme depends on the time-step $\mathrm{d}t_{DE}$ used for the time discretization. $\mathrm{d}t_{DE}$ should be smaller than a critical time-step determined such that the DE algorithm can describe the propagation of an elastic wave in the mass-spring system constituted by the solid granular assembly.

2.2 The Lattice Boltzmann method (LB)

To simulate fluid flow, we developed a two-dimensional Lattice Boltzmann algorithm (Lominé et al. 2010). With the LB method, the entire domain is spatially discretized using a regular square lattice of step h. In this work the D2Q9 discretization model (Qian et al. 1992) is used. With this model, for each lattice node located at position $\boldsymbol{x}$, nine directions i and nine discrete velocities

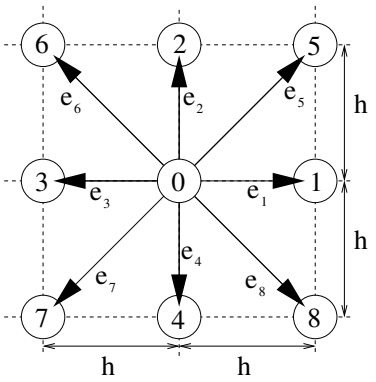

Fig. 2. D2Q9 model: discrete velocity directions from a node located at position $\boldsymbol{x}$.

$\boldsymbol{e_i}$ are defined, pointing towards the eight first neighbour nodes located at positions $\boldsymbol{x} + \boldsymbol{e_i}\mathrm{d}t$ as illustrated in Fig. 2.

Here $\mathrm{d}t$ is the time-step of the LB algorithm and discrete velocities can be expressed as follows:

$$\boldsymbol{e}_i = \begin{cases} (0,0) & \text{if } i = 0 \\ C\left(\cos\left(\frac{\pi(i-1)}{2}\right), \sin\left(\frac{\pi(i-1)}{2}\right)\right) & \text{for } i = 1,\ldots,4 \\ C\left(\cos\left(\frac{\pi(2i-9)}{4}\right), \sin\left(\frac{\pi(2i-9)}{4}\right)\right) & \text{for } i = 5,\ldots,8 \end{cases} \tag{1}$$

where $C = h/\mathrm{d}t$ is the lattice velocity. For a node located at position $\boldsymbol{x}$, a density distribution function $f_i(\boldsymbol{x}, t)$ is associated with each direction i, representing the number of fluid particles moving along the direction i with the velocity $\boldsymbol{e_i}$. The Lattice Boltzmann method can be divided into two consecutive steps: the collision and streaming steps. During the collision step, particle distribution functions relax towards equilibrium functions f_i^{eq}. This relaxation is performed here with the single-relaxation Bhatnagar-Gross-Krook (BGK) model (Bhatnagar et al. 1954):

$$f_i(\boldsymbol{x}, t^+) = f_i(\boldsymbol{x}, t) - \frac{1}{\lambda}\left[f_i(\boldsymbol{x}, t) - f_i^{eq}(\boldsymbol{x}, t)\right] \tag{2}$$

where λ is a dimensionless relaxation time linked to the kinematic viscosity of the fluid ν, the lattice velocity C, and the lattice spacing h through the relation $\nu = \frac{1}{3}\left(\lambda - \frac{1}{2}\right)Ch$. $f_i(\boldsymbol{x}, t^+)$ is called the post-collision term since it refers to particle distribution functions following the collision step.

For Newtonian fluid, the equilibrium distribution functions write (Qian et al. 1992):

$$f_i^{eq} = w_i\rho\left(1 + \frac{3}{C^2}\boldsymbol{e_i}.\boldsymbol{v} + \frac{9}{2C^4}(\boldsymbol{e_i}.\boldsymbol{v})^2 - \frac{3}{2C^2}\boldsymbol{v}.\boldsymbol{v}\right) \text{ for } i = 0,\ldots,8 \tag{3}$$

where $w_0 = 4/9$, $w_{1,2,3,4} = 1/9$ and $w_{5,6,7,8} = 1/36$. $\boldsymbol{v}$ and ρ are respectively the macroscopic fluid velocity and density at the considered node. They are determined with the following relations:

$$\rho = \sum_{i=0}^{8} f_i \text{ and } \boldsymbol{v} = \frac{1}{\rho}\sum_{i=0}^{8} f_i\boldsymbol{e_i} \tag{4}$$

The fluid pressure p is linked to fluid density using the equation of state $p = c_s^2\rho$, where $c_s = \frac{C}{\sqrt{3}}$ is the sound celerity. Macroscopic quantities converge on the solution of the incompressible Navier-Stokes equation with order M^2, where $M = v_{max}/C$ is the computational Mach

number and v_{max} the maximum fluid velocity. We used a value of $M \leq 0.1$, which leads to a compressibility error M^2 less than 1%.

During the streaming step, all distribution functions resulting from the collision process are propagated along each direction to the nearest neighbour node. With notations previously defined, this step can simply be written as:

$$f_i(\boldsymbol{x} + \boldsymbol{e_i}\mathrm{d}t, t + \mathrm{d}t) = f_i(\boldsymbol{x}, t^+) \tag{5}$$

Solid obstacles in the LB method are taken into account by placing them on the lattice. This discretization of solid obstacles leads to differentiate solid nodes (the nodes belonging to the solid obstacles), fluid nodes (nodes that do not belong to solid obstacles), solid boundary nodes (solid nodes representing an obstacle surface with at least one velocity direction pointing towards a fluid node) and fluid boundary nodes (fluid nodes with at least one velocity direction pointing towards a solid boundary node). In this paper, solid boundary nodes and fluid boundary nodes will be referred respectively as SB nodes and FB nodes. In the streaming step, fluid particles are not allowed to cross obstacle boundaries. Therefore, distribution functions coming from an FB node and propagating towards a SB node are reflected according to the following modified bounce-back rule (Ladd 1994):

$$f_{-\sigma i}(\boldsymbol{x}_{FB}, t + \mathrm{d}t) = f_{\sigma i}(\boldsymbol{x}_{FB}, t^+) - 2\alpha_i \boldsymbol{V_b}.\boldsymbol{e_i} \tag{6}$$

In equation (6), $\boldsymbol{x}_{FB}$ is the position of the FB node; σi is the direction from the FB node to the SB node constituting a boundary link; α_i is a constant defined by $\alpha_i = 3w_i\rho C^2$, and $\boldsymbol{V_b}$ is the solid boundary velocity at the middle of the boundary link σi.

Hydrodynamic force $\boldsymbol{F}_\sigma$ and torque $\boldsymbol{T}_\sigma$ contributions coming from each boundary link, are evaluated from the momentum exchange between fluid and solid particle surface (Ladd 1994; Mei et al. 2002). In two dimensions, these contributions write:

$$\boldsymbol{F}_\sigma(\boldsymbol{x}, t + \frac{1}{2}\mathrm{d}t) = 2\frac{h^2}{\mathrm{d}t}\left[f_{\sigma i}(\boldsymbol{x}, t^+) - \alpha_i \boldsymbol{V_b}.\boldsymbol{e_i}\right]\boldsymbol{e}_{\sigma i} \tag{7}$$

$$\boldsymbol{T}_\sigma(\boldsymbol{x}, t + \frac{1}{2}\mathrm{d}t) = \boldsymbol{r}_c \times \boldsymbol{F}_\sigma(\boldsymbol{x}, t + \frac{1}{2}\mathrm{d}t) \tag{8}$$

where $\boldsymbol{r}_c$ is the vector joining the centre of mass of the solid particle to the middle of the boundary link. The total hydrodynamic force and torque applied on a solid particle at time t are obtained by summing equations (7) and (8) respectively over all boundary links of the particle and by averaging the results over two consecutive LB time-steps.

2.3 Coupling between DE and LB methods.

In most situations, the time-step of the DE method is smaller than the time-step of the LB method. Therefore, the coupling is based on a subcycling scheme. During one loop of the LB method, n loops of the DE method are performed. To achieve a such subcycling, the DE time-step is set to satisfy the relation $\mathrm{d}t = n\mathrm{d}t_{DE}$ together with the condition of stability of the explicit time integration achieved during DE loop. To resume, positions and velocities of particles are computed with the DE method. Then, these particles are mapped on the LB lattice, and their positions and velocities constitute input parameters for the LB method to calculate hydrodynamic

forces and torques. These latter are added to inter-particle forces and torques determined by the DE method to compute new particle positions and velocities.
We used an open source software, named YADE (Kozicki & Donzé 2008), dedicated to the DE method. This software is designed in such a way that contact laws or functionalities are incorporated with plugins. Therefore, we developed a plugin to calculate hydrodynamic forces and torques with the Lattice Boltzmann method and integrated it into the YADE software.

2.4 Model set-up

We applied the coupled DE/LB method presented previously to the study of piping erosion. As explained previously, our numerical set-up is inspired by the Hole Erosion Test (HET), but it is here limited to the two-dimensional case. A rectangular box of length l is filled up with a packing of cohesive frictional disks of diameter d with a size dispersion of 30%. A schematic drawing is given in Fig. 3. The initial hole with inlet and outlet water chambers are created by

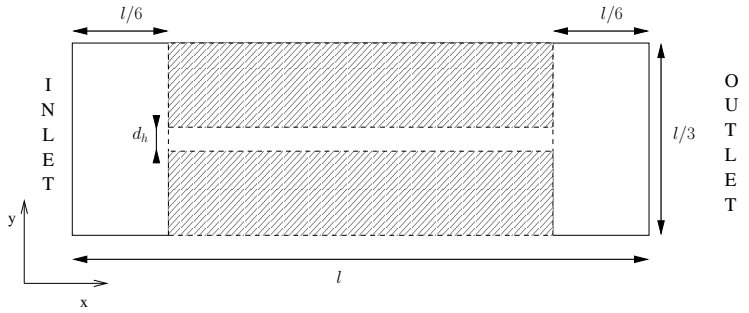

Fig. 3. Schematic representation of the numerical set-up used to simulate erosion through a pipe: $l = 0.03$ m, $d_{\text{mean}} = 5.06\ 10^{-4}$ m, $d_h = 0.2 \times l/3$. Hatched regions correspond to the locations of the cohesive material after drilling of the granular assembly.

removing grains that are not in the hatched regions as represented in Fig. 3. We also removed the left and right walls and the system is saturated with water ($\nu = 1\ 10^{-6}$ m^2 s^{-1} and $\rho_0 = 1\ 000$ kg m^{-3}). Then, a pressure gradient ΔP between the inlet and the outlet is applied, $\Delta P = p_{\text{in}} - p_{\text{out}} = c_s^2(\rho_{\text{in}} - \rho_{\text{out}})$. Nevertheless, pressure or velocity boundary conditions cannot be directly imposed on the system boundaries. These macroscopic quantities depend on the distribution functions. On system boundaries, these distribution functions have to be set to match the desired value of the fluid pressure or velocity. This is achieved on the basis of the boundary conditions defined by Zou and He (1997). For the two remaining upper and bottom walls, a zero velocity boundary condition is imposed. The DE and LB parameters used in this work are the following: $\lambda = 1.1$, $C_s/d = -C_n/d = 0.25$; 1.01 and 2.53 N m^{-1}, $k_n/d = 150\ 10^6$ N m^{-2}, $k_s/k_n = 0.4$, $\Phi = 20\,^\circ$.

3 RESULTS AND DISCUSSION

We simulated flows through the pipe described in section 2.4 for a given pressure gradient and different inter-particle cohesions. The pressure gradient applied is $\Delta P = 0.2$ Pa, corresponding to an hydraulic gradient $i = 3\Delta P/(\rho_0 g 2l) = 10\ 10^{-4}$, (where $g = 9.81$ m s^{-2} is the gravitational acceleration). Three cohesion values were considered: $C_s/d = -C_n/d = 0.25$; 1.01 and 2.53 N m^{-1}.

Fig. 4 shows snapshots from the simulation for $C_s/d = -C_n/d = 0.25$ N m^{-1}. These snapshots highlight that piping erosion can be simulated with the coupled method presented previ-

ously. Indeed, it is possible to observe the detachment and the transport of particles through the pipe due to the fluid flow.

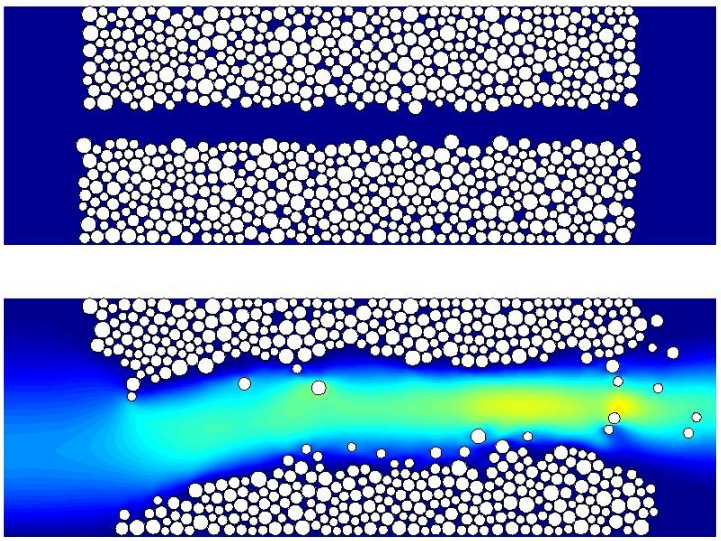

Fig. 4. Snapshots from a simulation of piping erosion obtained with the coupling between the DE and LB methods, for $i = 10\ 10^{-4}$ and $C_s/d = -C_n/d = 0.25$ N m^{-1}. The colour gradient is proportional to the fluid velocity.

Particles reaching the outlet are removed and are considered as eroded ones. During simulations, we record the eroded particle mass $M_e(t)$. Figure 5 represents the evolution of the ratio $M_e(t)/M_0$ with time, where M_0 is the total mass of the initial granular assembly.

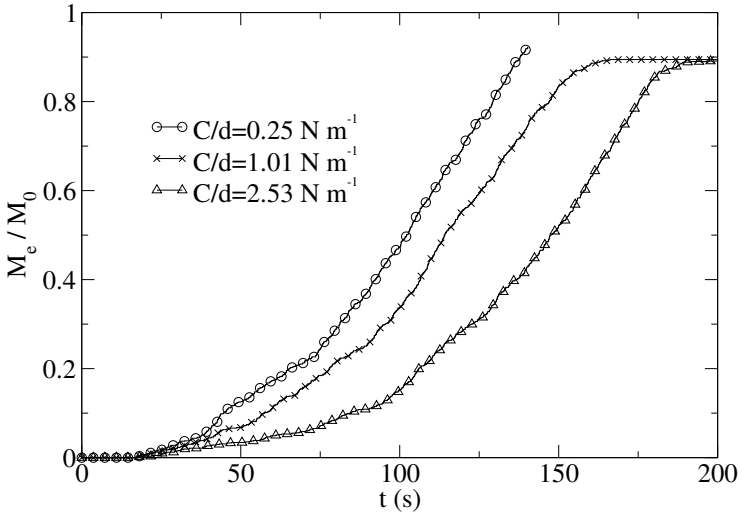

Fig. 5. Evolution of the ratio M_e/M_0 with time for different values of $C/d = C_s/d = -C_n/d$.

Figure 5 illustrates that the proportion of eroded particle mass increases with time. At the end of simulations the ratio $M_e(t)/M_0$ reaches a limit value smaller than 1 because some of the last particles, stuck to the upper and bottom walls, cannot be removed by the water flow. For the inter-particle cohesion values considered, the increase of the cohesion tends to delay the erosion

process, but not to limit it. After a given time, greater for higher cohesion values, the whole granular assembly is eroded.

A classical parameter used to evaluate the importance of the erosion process at a given time is the rate of eroded mass per unit pipe area $\dot{\epsilon}$, displayed in Fig. 6. For all cohesion values the erosion rate increases with time, highlighting the development of the kinetic of erosion as the pipe expands. At the end of simulations, erosion rate decreases due to the vanishing of granular material stock. This last tendency is not representative of the characteristics of erodability of the granular material, and only the first increasing part of erosion rate is considered later on in the paper.

Once again, the cohesion of the granular assembly has a direct influence on the erosion process by delaying the development of the kinetic of erosion.

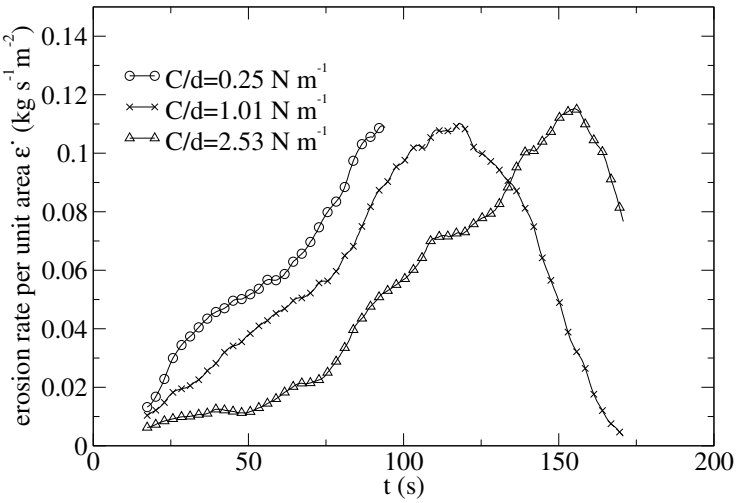

Fig. 6. Evolution of the rate of eroded mass $\dot{\epsilon}$ with time for different values of $C/d = C_s/d = -C_n/d$.

A commonly erosion law used and retrieved in HET (Wan & Fell 2004; Pham 2008) is a linear dependency of the rate of eroded mass on the hydraulic shear stress:

$$\dot{\epsilon} = k_d \left(\tau - \tau_c\right) \text{if } \tau > \tau_c, \tag{9}$$

where k_d is the erosion coefficient, τ is the fluid shear stress and τ_c is a critical shear stress.

Experimentally, the evaluation of the shear stress is based on the hole diameter measurement and on the pressure gradient imposed. Considering an equilibrium between pressure forces and shear forces in a two dimensional pipe of height $2R$ and length L, it comes:

$$\tau = \frac{R\Delta P}{L} \tag{10}$$

Contrary to previous experiments performed by Wan & Fell (2004), where only initial and final hole diameter where known, our simulations let us access to the hole diameter at any time during the piping erosion process. Here, we determined the mean hole diameter from an averaged cross-section density profile over the entire packing of disks. τ is calculated using equation (10) until the ratio between the hole diameter and the channel height is greater than 75%, to avoid influence of vanishing of granular material stock.

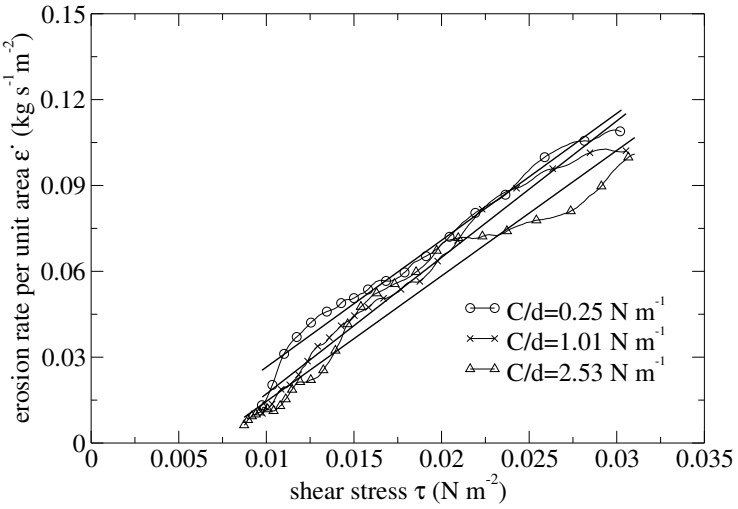

Fig. 7. Evolution of the rate of eroded mass $\dot{\epsilon}$ with the fluid shear stress τ, for different values of $C/d = C_s/d = -C_n/d$.

Figures 7 presents dependency of $\dot{\epsilon}$ on shear stress τ. Three least squares linear adjustments are also represented and illustrate that the erosion law classically used in HET can be retrieved with our simulations of piping erosion with the coupled LB-DE method.

However, the influence of the inter-particle cohesion on the development of the erosion process, shown in Figs. 5 and 6, is not clearly visible in a such representation. Approximatively the same linear relation between $\dot{\epsilon}$ and τ is found for the three cohesion values. Consequently it would mean, according to the erosion law expressed by equation (9), that the three granular assemblies with different cohesions have similar characteristics of erodability. This last point still constitutes for us an open question. Does the way used here, to estimate the fluid shear stress, allow to characterize properly the loading applied by the fluid on solid particles? Is, the fluid shear stress the only fluid parameter fixing the erosion regime, for our set-up and numerical granular material?

4 CONCLUSION

In this paper, a coupling between the Discrete Element method and the Lattice Boltzmann method was presented. In a such coupling few hypotheses are introduced in the modelling of fluid flow, solid particle interactions and fluid-solid interaction, avoiding any phenomenological description. This point constitutes a good advantage, and only six input mechanical parameters are used in this model: the fluid viscosity, the normal and tangential contact stiffnesses and cohesions between two solid particles, and finally the inter-particle friction angle.

Simulations of piping erosion through a granular assembly shown that an erosion law classically used to describe hole erosion tests can be retrieved with this numerical coupled method: the erosion rate is proportional to the fluid shear stress. It is shown, that the inter-particle cohesion influence the kinetic of erosion by delaying the erosion process. However, this influence of cohesion disappears when the erosion rate is expressed with respect to the fluid shear stress. More investigations are necessary to validate this last point or to suggest another interpretation.

ACKNOWLEDGEMENTS

We would like to gratefully acknowledge the French Region Pays de la Loire for its financial support through the EMERMOD project.

REFERENCES

Bhatnagar, P., Gross, E., & Krook, M. (1954). A model for collision processes in gases. I. Small amplitude processes in charged and neutral one-component systems. *Physical Review 94*(3), 511–525.

Cundall, P. A. & Strack, O. D. L. (1979). A discrete numerical model for granular assemblies. *Geotechnique 29*(1), 47–65.

Foster, M., Fell, R., & Spannagle, M. (2000). The statistics of embankment dam failures and accidents. *Canadian Geotechnical Journal 37*(5), 1000–1024.

Kozicki, J. & Donzé, F. V. (2008). A new open-source software developed for numerical simulations using discrete modeling methods. *Computer Methods in Applied Mechanics and Engineering 197*(49-50), 4429–4443.

Ladd, A. (1994). Numerical simulations of particulate suspensions via a discretized Boltzmann equation. Part 1. Theoretical foundation. *Journal of Fluid Mechanics 271*(1), 285–309.

Lominé, F., Scholtès, L., Poullain, P., & Sibille, L. (2010). Soil microstructure changes induced by internal fluid flow: investigations with coupled DE/LB methods. In I. Doghri, R. E. Fatmi, F. Darve, H. Hassis, & H. Zenzri (Eds.), *Third Euro-Mediterranean Symposium on Advances in Geomaterials and Structures*, Djerba, pp. 885–890.

Mei, R., Yu, D., Shyy, W., & Luo, L.-S. (2002). Force evaluation in the lattice Boltzmann method involving curved geometry. *Phys. Rev. E 65*(4), 41203.

Pham, T. (2008). *Erosion et dispersion des sols argileux par un fluide*. Ph. D. thesis, École Nationale des Ponts et Chaussées.

Qian, Y. H., D'Humieres, D., & Lallemand, P. (1992). Lattice BGK Models for Navier-Stokes Equation. *EPL (Europhysics Letters) 17*(6), 479–484.

Regazzoni, P.-L. (2009). *Confrontation et analyse d'érodimètres et caractérisation de la sensibilité à l'érosion d'interface.* Ph. D. thesis, Université de Nantes.

Wan, C. F. & Fell, R. (2004). Investigation of Rate of Erosion of Soils in Embankment Dams. *Journal of Geotechnical and Geoenvironmental Engineering 130*(4), 373–380.

Zou, Q. & He, X. (1997). On pressure and velocity boundary conditions for the lattice Boltzmann BGK model. *Physics of Fluids 9*(6), 1591–1598.